

Plasma Diagnostics in High-Resolution X-ray Spectra of Magnetic Cataclysmic Variables

Christopher W. Mauche

This article was submitted to
The Physics of Cataclysmic Variables and Related Objects,
Gottingen, Germany, Aug 6-10, 2001

U.S. Department of Energy

October 2, 2001

Lawrence
Livermore
National
Laboratory

DISCLAIMER

This document was prepared as an account of work sponsored by an agency of the United States Government. Neither the United States Government nor the University of California nor any of their employees, makes any warranty, express or implied, or assumes any legal liability or responsibility for the accuracy, completeness, or usefulness of any information, apparatus, product, or process disclosed, or represents that its use would not infringe privately owned rights. Reference herein to any specific commercial product, process, or service by trade name, trademark, manufacturer, or otherwise, does not necessarily constitute or imply its endorsement, recommendation, or favoring by the United States Government or the University of California. The views and opinions of authors expressed herein do not necessarily state or reflect those of the United States Government or the University of California, and shall not be used for advertising or product endorsement purposes.

This is a preprint of a paper intended for publication in a journal or proceedings. Since changes may be made before publication, this preprint is made available with the understanding that it will not be cited or reproduced without the permission of the author.

This work was performed under the auspices of the United States Department of Energy by the University of California, Lawrence Livermore National Laboratory under contract No. W-7405-Eng-48.

This report has been reproduced directly from the best available copy.

Available electronically at <http://www.doc.gov/bridge>

Available for a processing fee to U.S. Department of Energy
And its contractors in paper from
U.S. Department of Energy
Office of Scientific and Technical Information
P.O. Box 62
Oak Ridge, TN 37831-0062
Telephone: (865) 576-8401
Facsimile: (865) 576-5728
E-mail: reports@adonis.osti.gov

Available for the sale to the public from
U.S. Department of Commerce
National Technical Information Service
5285 Port Royal Road
Springfield, VA 22161
Telephone: (800) 553-6847
Facsimile: (703) 605-6900
E-mail: orders@ntis.fedworld.gov
Online ordering: <http://www.ntis.gov/ordering.htm>

OR

Lawrence Livermore National Laboratory
Technical Information Department's Digital Library
<http://www.llnl.gov/tid/Library.html>

Plasma Diagnostics in High-Resolution X-ray Spectra of Magnetic Cataclysmic Variables

Christopher W. Mauche

*Lawrence Livermore National Laboratory, L-43, 7000 East Avenue,
 Livermore, CA 94550*

Abstract. Using the *Chandra* HETG spectrum of EX Hya as an example, we discuss some of the plasma diagnostics available in high-resolution X-ray spectra of magnetic cataclysmic variables. Specifically, for conditions appropriate to collisional ionization equilibrium plasmas, we discuss the temperature dependence of the H- to He-like line intensity ratios and the density and photoexcitation dependence of the He-like R line ratios and the Fe XVII $I(17.10 \text{ \AA})/I(17.05 \text{ \AA})$ line ratio. We show that the plasma temperature in EX Hya spans the range from ≈ 0.5 to ≈ 10 keV and that the plasma density $n \gtrsim 2 \times 10^{14} \text{ cm}^{-3}$, orders of magnitude greater than that observed in the Sun or other late-type stars.

1. Introduction

In magnetic cataclysmic variables (mCVs), the flow of material lost by the secondary is channeled onto small spots on the white dwarf surface in the vicinity of the magnetic poles. Because the infall velocity is supersonic, the flow passes through a strong shock above the stellar surface, where 15/16 of its prodigious kinetic energy is converted into thermal energy. The post-shock plasma is hydrostatically supported, and cools via cyclotron, thermal bremsstrahlung, and line emission before settling onto the white dwarf surface. Consequently, the post-shock plasma of mCVs is both multi-temperature and multi-density, with a post-shock temperature $T \leq T_{\text{shock}} = 3GM_{\text{wd}}\mu m_{\text{H}}/8kR_{\text{wd}} \approx 250 \text{ MK} \approx 20 \text{ keV}$ and density $n \geq n_{\text{shock}} = \dot{M}/4\pi f R_{\text{wd}}^2 \mu m_{\text{H}} (v_{\text{ff}}/4) \approx 10^{13} \text{ cm}^{-3}$ for a mass-accretion rate $\dot{M} = 10^{15} \text{ g s}^{-1}$ (hence $L = GM_{\text{wd}}\dot{M}/R_{\text{wd}} \approx 9 \times 10^{31} \text{ erg s}^{-1}$), relative spot size $f = 0.1$, and free-fall velocity $v_{\text{ff}} = (2GM_{\text{wd}}/R_{\text{wd}})^{1/2} \approx 4300 \text{ km s}^{-1}$. If the shock height is a small fraction of the white dwarf radius, a significant fraction of the resulting X-ray emission is intercepted by the white dwarf surface. Competition between photoelectric absorption and Thompson and Compton scattering results in ~ 20 keV X-rays being predominantly scattered by the white dwarf photosphere, resulting in a hard reflection spectral component, while softer and harder X-rays are increasingly likely to deposit their energy in the white dwarf photosphere, heating it to a temperature $T_{\text{bb}} \approx (GM_{\text{wd}}\dot{M}/8\pi\sigma f R_{\text{wd}}^3)^{1/4} \approx 30 \text{ kK}$. \dot{M}/f must be larger by a factor of $\sim 10^4$ to explain the soft X-ray spectral component of AM Her-type mCVs.

The *unique* aspect of the X-ray-emitting plasma in mCVs is the high densities, which are the result of the magnetic funneling of the mass lost by the

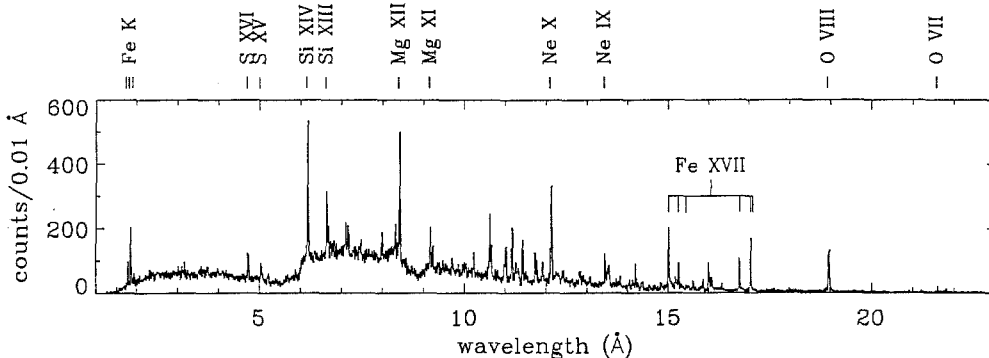


Figure 1. *Chandra* HEG ($\lambda < 3.5 \text{ \AA}$) and MEG ($\lambda \geq 3.5 \text{ \AA}$) count spectrum of EX Hya. Identifications are provided for emission lines of H- and He-like ions of O, Ne, Mg, Si, S, and Fe. Most other lines are due to Fe L-shell ions; those from Fe XVII are labeled.

secondary, the factor-of-four density jump across the accretion shock, and the settling nature of the post-shock flow, wherein the density $n \propto T^{-1}$. X-ray line intensity ratios have long been used to diagnose the temperature and density of solar plasma, but until recently the effective area and spectral resolution of X-ray observatories have been inadequate to allow similar studies of cosmic X-ray sources. The multi-temperature nature of the plasma in CVs is readily apparent from the broad-band nature of their X-ray continua, but even with the 0.5–10 keV bandpass and $\Delta E = 120 \text{ eV}$ spectral resolution of the *ASCA* SIS detectors, it is possible to adequately describe the observed spectra of CVs with a small number (typically 2) of discrete temperature components. Ishida, Mukai, & Osborne (1994) and subsequently Fujimoto & Ishida (1997) first applied the ratio of the intensities of the H- to He-like lines of Mg, Si, S, Ar, and Fe in the *ASCA* SIS spectrum of the intermediate polar-type mCV EX Hya to constrain the range of temperatures present in its accretion column. Unfortunately, *ASCA* did not have the spectral resolution necessary to utilize any of the *density* diagnostics available in the X-ray bandpass, such as the density-sensitive He-like triplets, which require $\Delta E \lesssim 60 \text{ eV}$. With the launch of the *Chandra* and *XMM-Newton* X-ray observatories, it is now possible to utilize a broad range of spectral diagnostics to characterize the plasma of mCVs.

2. *Chandra* HETGS Observation of EX Hya

Motivated by the beautiful *ASCA* spectrum, we recently obtained *Chandra* HETGS ($\Delta\lambda = 0.01$ and 0.02 \AA) and *XMM-Newton* RGS ($\Delta\lambda = 0.07 \text{ \AA}$) and EPIC spectra of EX Hya. The 60 ks *Chandra* observation was performed on 2000 May 18 during a multiwavelength (*RXTE*, *Chandra*, *EUVE*, *FUSE*, *HST*, and ground-based optical) campaign, while the *XMM-Newton* observation (100 ks) was performed on 2000 July 1–2. Because of space limitations, we discuss here only the *Chandra* HETG spectrum, which is shown in Figure 1. The spectrum consists of a modest continuum with superposed lines of H- and He-like O, Ne,

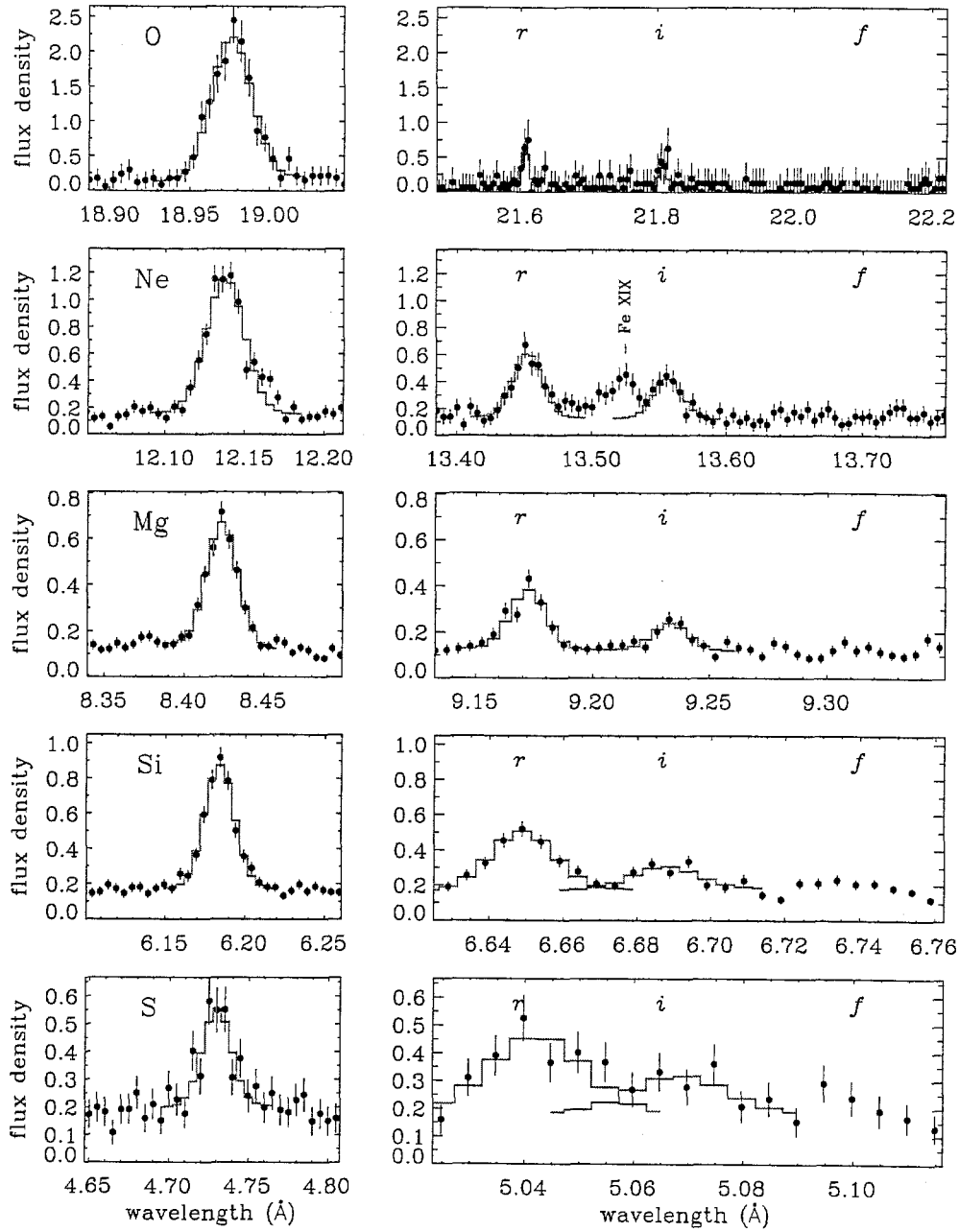


Figure 2. Detailed views of the H-like Ly α and He-like triplet lines of O, Ne, Mg, Si, and S in the MEG spectrum of EX Hya. Units of flux density are 10^{-2} photons cm^{-2} s^{-1} \AA^{-1} . Data are shown by the filled circles with error bars, Gaussian fits (broadened by the spectrometer resolution) are shown by the gray histograms. Positions of the resonance (*r*), intercombination (*i*), and forbidden (*f*) lines of the He-like triplets are indicated. Note the absence of the forbidden lines, indicating high electron densities and/or photoexcitation.

Mg, Si, S, and Fe; Fe XVII–XXIV; and “neutral” Fe (via the weak fluorescent line at $6.4 \text{ keV} = 1.94 \text{ \AA}$). Whereas the optical–FUV emission lines of EX Hya are *broad*, with $\text{FWHM} \approx 7\text{--}10 \text{ \AA} \sim 2000\text{--}3000 \text{ km s}^{-1}$ (Hellier et al. 1987; Greeley et al. 1997; Mauche 1999), the X-ray emission lines are *narrow*, with $\text{FWHM} \approx 20 \text{ m\AA} \sim 600 \text{ km s}^{-1}$. This is explained qualitatively by the fact that (1) the post-shock velocity $v \leq v_{\text{shock}} = v_{\text{ff}}/4 \approx 900 \text{ km s}^{-1}$ and (2) we view the EX Hya binary nearly edge-on, so the velocity vector of the post-shock flow lies more nearly on the plane of the sky.

3. Temperature Diagnostic

As was done with the *ASCA* spectra, we can use the ratio of the H- to He-like line intensities in the HETG spectrum of EX Hya to constrain the temperature distribution in the post-shock plasma. This was accomplished by fitting Gaussians to the various emission lines, accounting for the effective area and resolution function of the spectrometer. Results of these fits are shown in Figure 2 for O, Ne, Mg, Si, and S. In addition to easily resolving the H- and He-like emission lines, the HETGS cleanly resolves the resonance (*r*), intercombination (*i*), and forbidden (*f*) lines of the He-like triplets, as well as accounts for the presence of other emission lines, such as the relatively strong Fe XIX emission line situated between the resonance and intercombination lines of Ne IX (these three lines appear as a blob in the *XMM* RGS spectrum). Assuming the Mewe, Gronenschild, & van den Oord (1985) collisional ionization equilibrium (CIE) ionization balance and line intensities, Figure 3 shows that the measured H- to He-like line intensity ratios require that the plasma temperature extends from $kT_{\text{min}} \approx 0.5 \text{ keV}$ to $kT_{\text{max}} \approx 10 \text{ keV}$. This is the same range inferred by Fujimoto & Ishida (1997) from the *ASCA* spectrum of EX Hya, even though the SIS could not resolve the H- and He-like emission lines of O and Ne. The lower temperature limit is a bit of a puzzle, because it seems inescapable that the plasma will cool below this temperature. A possible explanation is that the optical depths in the lines begins to be important at this temperature, where the plasma density is expected to be a factor of $\sim T_{\text{max}}/T_{\text{min}} \sim 20$ times higher than the value just below the accretion shock.

4. Density Diagnostics

4.1. He-like R Line Ratios

The standard density diagnostic of high-temperature plasmas is the ratio of the forbidden to intercombination lines of He-like ions (Gabriel & Jordan 1969; Blumenthal, Drake, & Tucker 1972; Porquet et al. 2001). Because the $1s2s^3S_1$ upper level of the forbidden line is metastable, it can be depopulated by collisional excitation, leading to the conversion of the $1s^21S_0\text{--}1s2s^3S_1$ forbidden line *f* into the $1s^21S_0\text{--}1s2p^3P_{2,1}$ intercombination blend *i* (for the Grotrian diagram, refer to the left panel of Fig. 4). We used the LXSS plasma code being developed at LLNL (Mauche, Liedahl, & Fournier 2001) to calculate the $R \equiv f/i$ line ratios as a function of electron density for the abundant elements, and present the results in Figure 5. It can be seen that the critical density for this ratio

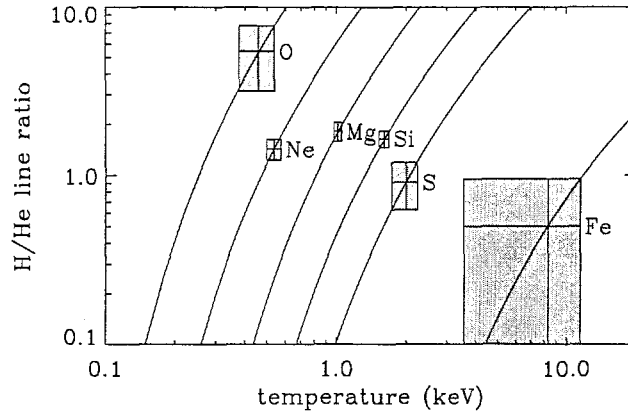


Figure 3. Temperature distribution of the plasma in EX Hya based on the measured H- to He-like line intensity ratios. Curves assume the Mewe, Gronenschild, & van den Oord (1985) CIE ionization balance and line intensities, and the error boxes are 1σ based on counting statistics alone. A broad range of temperatures is indicated, from $kT_{\min} \approx 0.5$ keV (probably the temperature where the optical depth in the lines becomes important) to $kT_{\max} \approx 10$ keV (comparable to the shock temperature $T_{\text{shock}} = 15.4^{+5.3}_{-2.6}$ keV inferred by Fujimoto & Ishida 1997 from the *ASCA* SIS spectrum of EX Hya).

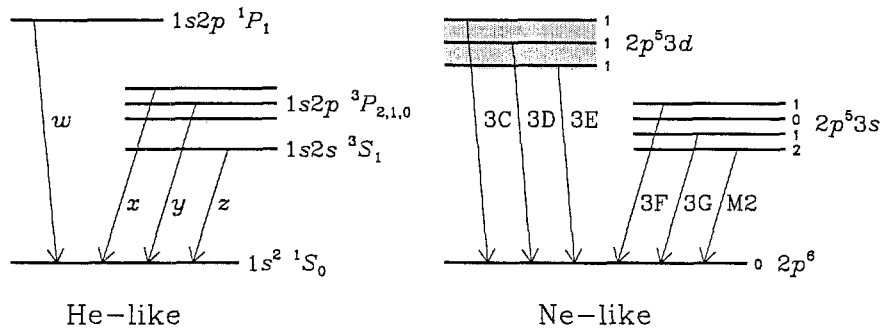


Figure 4. Simplified Grotrian diagrams for He- and Ne-like ions. For the He-like diagram the resonance ($w = r$), intercombination ($x+y = i$) and forbidden ($z = f$) lines are labeled. For the Ne-like diagram the 3C–M2 lines are labeled; for Fe XVII these correspond to the $\lambda = 15.01$, 15.26, 15.45, 16.78, 17.05, and 17.10 Å lines, respectively, indicated in Fig. 1.

scales with Z , ranging from $n_c \approx 6 \times 10^8 \text{ cm}^{-3}$ for C to $n_c \approx 3 \times 10^{17} \text{ cm}^{-3}$ for Fe. Unfortunately, this trend is opposite to that in the accretion column of mCVs (where the high- Z ions dominate at the top of the column where the temperature is highest and the density is lowest, and the low- Z ions dominate at the bottom of the column where the temperature is lowest and the density is highest), limiting our ability to “map” the density structure of the column. As is evident from Figure 2, all the He-like triplets of EX Hya are in the “high-density limit” ($R \approx 0$), implying that the plasma density $n_e \gtrsim 10^{15} \text{ cm}^{-3}$.

4.2. Complications from Photoexcitation

Unfortunately, this result is not entirely secure. In UV-bright sources like early-type stars, X-ray binaries, and CVs, photoexcitation as well as collisional excitation acts to depopulate the upper level of the He-like forbidden lines. If the radiation field is sufficiently strong at the appropriate wavelengths, the R line ratio can be in the “high-density limit” regardless of the density. Photoexcitation has been shown to explain the low R line ratios of early-type stars (Kahn et al. 2001; Waldron & Cassinelli 2001), and could explain the low R line ratios of EX Hya. To investigate this effect, we included in the LXSS level-population kinetics calculation the photoexcitation rates $(\pi e^2/m_e c) f_{ij} F_\nu(T)$, where $F_\nu(T)$ is the continuum spectral energy distribution and f_{ij} are the oscillator strengths of the various transitions. For simplicity, we assume that $F_\nu(T) = (4\pi/h\nu) B_\nu(T_{\text{bb}})$ (i.e., the radiation field is that of a blackbody of temperature T_{bb}) and that the dilution factor of the radiation field is equal to $\frac{1}{2}$ (i.e., the X-ray-emitting plasma is in close proximity to the source of the photoexcitation continuum). For $T_{\text{bb}} = 30 \text{ kK}$, we obtain the R line ratios shown by the full curves in the right panel of Figure 5, which demonstrates that, for the given assumptions, all of the He-like R line ratios through Si XIII are significantly affected by photoexcitation. It is unfortunate that this affect begins to disappear at S XV, where the HETGS effective area is low and the spectral resolution is only just sufficient to resolve the He-like triplet. Calorimeter-type detectors like those planned for *Astro-E2* and *Constellation-X* are required to work at these short wavelengths/high energies.

4.3. Fe XVII I(17.10 Å)/I(17.05 Å) Line Ratio

Other than the H- and He-like lines of the abundant elements, the brightest emission lines in the *Chandra* HETG spectrum of EX Hya are the $2p^6-2p^53l$ ($l = s, d$) lines of Fe XVII at 15–17 Å (Fig. 1). These lines are strong in the X-ray spectra of high-temperature CIE plasmas because of the high abundance of Fe, the persistence of Ne-like Fe over a broad temperature range ($T_e \approx 2\text{--}12 \text{ MK}$), and the large collision strengths for $2p \rightarrow nd$ transitions. The importance of Fe XVII has engendered numerous studies of its atomic structure and level-population kinetics, and while emphasis is usually placed on the *temperature* dependence of the $2p-3l$ line ratios (e.g., Rugge & McKenzie 1985; Smith et al. 1985; Raymond & Smith 1986), Mauche, Liedahl, & Fournier (2001) recently discussed the *density* dependence of these ratios.

The Grotrian diagram for Fe XVII is shown in the right panel of Figure 4. Like the $1s2s\ ^3S_1$ upper level of the forbidden line of He-like ions, the $2p^53s$ ($J = 2$) upper level of the 17.10 Å line of Fe XVII is metastable, so

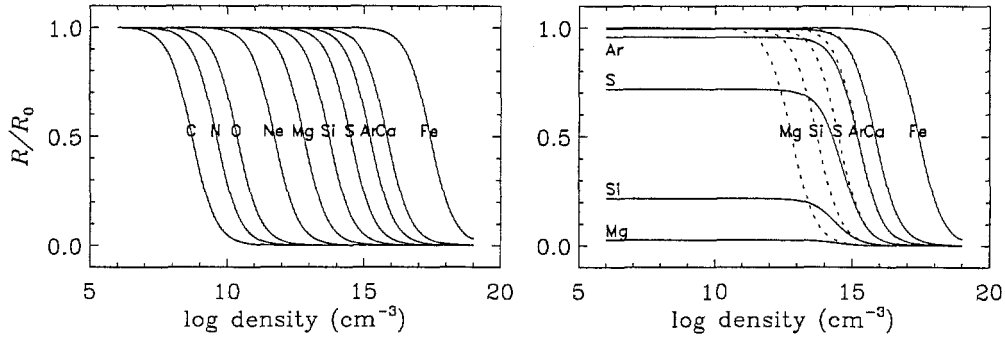


Figure 5. *Left panel:* He-like $R \equiv z/(x + y) = f/i$ line ratios of the abundant elements as a function of electron density. For C, N, O, ..., Fe, the plasma temperature $T_e = 0.46, 0.57, 0.86, \dots, 36.1$ MK, the temperature of the peak ionization fraction for each He-like ion. *Right panel:* Similar to the left panel (*dotted curves*), but accounts for photoexcitation by a $T_{bb} = 30$ kK blackbody (*full curves*). The R line ratios of all ions though Mg are in the “high-density limit” regardless of the density. In both panels the line ratios are scaled to the low-density values R_0 for ease of comparison.

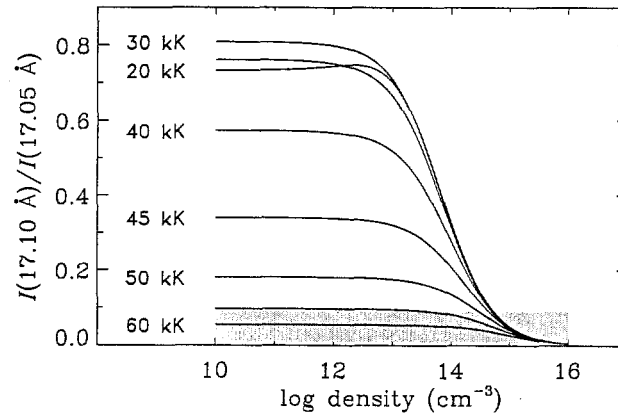


Figure 6. Fe XVII $I(17.10 \text{ \AA})/I(17.05 \text{ \AA})$ line ratio as a function of electron density for a $T_e = 4$ MK plasma photoexcited by a $T_{bb} = 20, 30, 35, 40, 45, 50, 55,$ and 60 kK blackbody. The gray stripe delineating the 1σ envelope of the line ratio measured in EX Hya requires that the electron density $n_e \gtrsim 3 \times 10^{14} \text{ cm}^{-3}$ and/or the blackbody temperature $T_{bb} \gtrsim 55$ kK.

collisional depopulation sets in at lower densities, and the intensity ratio of the 17.10 Å line to any of the other $2p$ - $3l$ lines (say, the 17.05 Å line) provides a diagnostic of the plasma density. The Fe XVII $I(17.10 \text{ Å})/I(17.05 \text{ Å})$ density diagnostic is ideal for mCVs for two reasons. First, the critical density is high: $n_c \approx 3 \times 10^{13} \text{ cm}^{-3}$, comparable to that of Si XIII. Second, the $I(17.10 \text{ Å})/I(17.05 \text{ Å})$ line ratio is less sensitive than the He-like R line ratios to photoexcitation. In Fe XVII, photoexcitations out the $2p^5 3s$ ($J = 2$) level go primarily into the $2p^5 3p$ manifold, requiring a significant flux of photons in the 190–410 Å waveband. In He-like ions, photoexcitations out the $1s2s \ ^3S_1$ level go primarily into the $1s2p \ ^3P_{2,1}$ levels, requiring a significant flux of photons at $\lambda = 1623, 1263, 1036, 865, 743, 637, 551, \text{ and } 404 \text{ Å}$ for O, Ne, Mg, Si, S, Ar, Ca, and Fe, respectively. Because the photoexcitation continuum is typically stronger in the UV–FUV than in the EUV, the Fe XVII $I(17.10 \text{ Å})/I(17.05 \text{ Å})$ line ratio is less sensitive to photoexcitation.

To investigate the density, temperature, and photoexcitation sensitivity of the Fe XVII $I(17.10 \text{ Å})/I(17.05 \text{ Å})$ line ratio, we calculated LXSS atomic models of Fe XVII for a range of densities $n_e = 10^{10}$ – 10^{16} cm^{-3} , temperatures $T_e = 2$ – 8 MK (spanning the range for which the Fe XVII ionization fraction is $\gtrsim 0.1$), and blackbody photoexcitation temperatures $T_{\text{bb}} = 20$ – 60 kK . The $I(17.10 \text{ Å})/I(17.05 \text{ Å})$ line ratio for $T_e = 4 \text{ MK}$, the peak of the Fe XVII ionization fraction, is shown in Figure 6. The measured Fe XVII $I(17.10 \text{ Å})/I(17.05 \text{ Å})$ line ratio of 0.05 ± 0.04 can be explained if the plasma density $n_e \gtrsim 3 \times 10^{14} \text{ cm}^{-3}$ or if the photoexcitation temperature $T_{\text{bb}} \gtrsim 55 \text{ kK}$. As detailed by Mauche, Liedahl, & Fournier (2001), the second option is consistent with the assumptions (blackbody emitter, dilution factor equal to $\frac{1}{2}$) and the observed FUV flux density only if the fractional emitting area of the accretion spot $f \leq 2\%$. This constraint and the observed X-ray flux requires a density $n \gtrsim 2 \times 10^{14} \text{ cm}^{-3}$ for the post-shock flow. Either way, then, the *Chandra* HETG spectrum of EX Hya requires that the plasma density in this mCV is orders of magnitude greater than that observed in the Sun or other late-type stars.

5. Summary

Using the *Chandra* HETG spectrum of EX Hya as an example, we have discussed some of the plasma diagnostics available in high-resolution X-ray spectra of mCVs. Specifically, we have discussed the temperature dependence of the H- to He-like line intensity ratios and the density and photoexcitation dependence of the He-like R line ratios and the Fe XVII $I(17.10 \text{ Å})/I(17.05 \text{ Å})$ line ratio. Since the discussion assumes that the plasma is in collisional ionization equilibrium and that the optical depths in the lines are negligible, it does *not* apply to (1) the pre-shock flow, where photoionization competes with collisional ionization to determine the physical state of the plasma, (2) the immediate post-shock flow, where the ions and electrons are not in thermal equilibrium, or (3) the very base of the post-shock flow, where the line optical depths are non-negligible. Where the plasma is optically thin and in collisional ionization equilibrium, the plasma temperature spans the range from ≈ 0.5 to $\approx 10 \text{ keV}$ and the plasma density $n \gtrsim 2 \times 10^{14} \text{ cm}^{-3}$. The lower temperature probably signals where the plasma

becomes optically thick in the lines, while the higher temperature is comparable to the shock temperature, which Fujimoto & Ishida (1997) inferred from the *ASCA* SIS spectrum of EX Hya is $T_{\text{shock}} = 15.4^{+5.3}_{-2.6}$ keV.

This communication has only scratched the surface of the many plasma diagnostics available in high-resolution X-ray spectra of mCVs. For lack of space, our discussion has concentrated on density diagnostics and the complicating affects of photoexcitation because these features are unique to mCVs. For a more general discussion of the physics of high-temperatures plasmas, the reader is referred to the volume "X-ray Spectroscopy in Astrophysics" (van Paradijs & Bleeker 1999), and particularly the chapters by R. Mewe and D. Liedahl.

Acknowledgments. We are indebted to D. Liedahl for his significant contributions to this work, and thank H. Tananbaum for the generous grant of Director's Discretionary Time which made the *Chandra* observations possible. Support for this work was provided in part by NASA Long-Term Space Astrophysics Program grant S-92654-F and NASA *Chandra* Guest Observer grant NAS8-39073. This work was performed under the auspices of the U.S. Department of Energy by University of California Lawrence Livermore National Laboratory under contract No. W-7405-Eng-48.

References

- Blumenthal, G. R., Drake, G. W. F., & Tucker, W. H. 1972, *ApJ*, 172, 205
 Fujimoto, R., & Ishida, M. 1997, *ApJ*, 474, 774
 Gabriel, A. H., & Jordan, C. 1969, *MNRAS*, 145, 241
 Greeley, B. W., Blair, W. P., Long, K. S., & Knigge, C. 1997, *ApJ*, 488, 419
 Hellier, C., Mason, K. O., Rosen, S. R., & Córdova, F. A. 1987, *MNRAS*, 228, 463
 Ishida, M., Mukai, K., & Osborne, J. P. 1994, *PASJ*, 46, L81
 Kahn, S. M., et al. 2001, *A&A*, 365, L312
 Mauche, C. W. 1999, *ApJ*, 520, 822
 Mauche, C. W., Liedahl, D. A., & Fournier, K. B. 2001, *ApJ*, 560, in press (astro-ph/0106518)
 Mewe, R., Gronenschild, E. H. B. M., & van den Oord, G. H. J. 1985, *A&AS*, 62, 197
 Porquet, D., Mewe, R., Dubau, J., Raassen, A. J. J., & Kaastra, J. S. 2001, *A&A*, 376, 1113
 Raymond, J. C., & Smith, B. W. 1986, *ApJ*, 306, 762
 Rugge, H. R., & McKenzie, D. L. 1985, *ApJ*, 297, 338
 Smith, B. W., Raymond, J. C., Mann, J. B., & Cowan, R. D. 1985, *ApJ*, 298, 898
 van Paradijs, J., & Bleeker, J. A. M. 1999, *X-ray Spectroscopy in Astrophysics* (Berlin: Springer)
 Waldron, W. L., & Cassinelli, J. P. 2001, *ApJ*, 548, L45

